An Integrated View of the Influence of Temperature, Pressure, and Humidity on the Stability of Trimorphic Cysteamine Hydrochloride

Inès Gana[a,b], Maria Barrio[c], Carine Ghaddar[d], Béatrice Nicolaï[a], Bernard Do[d], Josep-Lluís Tamarit[c], Fathi Safta[b], Ivo B. Rietveld[a,*]

[a] Caractérisation des Matériaux Moléculaires à Activité Thérapeutique (CAMMAT), Faculté de Pharmacie, Université Paris Descartes, 4, Avenue de l'Observatoire, 75006 Paris, France

[b] Laboratoire de chimie analytique, Faculté de Pharmacie, Université de Monastir, rue Ibn Sina, 5000 Monastir, Tunisie

[c] Grup de Caracterització de Materials (GCM), Departament de Física i Enginyeria Nuclear, Universitat Politècnica de Catalunya, ETSEIB, Diagonal 647, 08028 Barcelona, Spain

[d] Etablissement Pharmaceutique de l'Assistance Publique-Hôpitaux de Paris, Agence Générale des Equipements et Produits de Santé, 7, rue du Fer à Moulin, 75005 Paris, France

* Corresponding author: ivo.rietveld@parisdescartes.fr, tel.: +33 1 53739675

Abstract

Understanding the phase behavior of pharmaceuticals is important for dosage form development and regulatory requirements, in particular after the incident with ritonavir. In the present paper, a comprehensive study of the solid-state phase behavior of cysteamine hydrochloride used in the treatment of radiation sickness, sickle cell anemia and nephropathic cystinosis, is presented employing (high-pressure) calorimetry, water vapor sorption, and X-ray diffraction as a function of temperature. A new crystal form ($I2/a$, form III) has been discovered and its structure has been solved by X-ray powder diffraction, while two other crystalline forms are already known. The relative thermodynamic stabilities of the commercial form I and of the newly discovered form III have been established; they possess an overall enantiotropic phase relationship, with form I stable at room temperature and form III stable above 37 °C. Its melting temperature was found at 67.3 ± 0.5 °C. Cysteamine hydrochloride is hygroscopic and immediately forms a concentrated saturated solution in water with a surprisingly high concentration of 47.5 mole% above a relative humidity of 35 %. No hydrate has been observed. A temperature – composition phase diagram is presented that has been obtained with the unary pressure – temperature phase diagram, measurements, and calculations. For development, form I would be the best form to use in any solid dosage form, which should be thoroughly protected against humidity.

Keywords: cysteamine hydrochloride, crystalline trimorphism, phase diagram, phase stability, enantiotropic phase relationship, thermal expansion, intermolecular interactions, hygroscopic, eutectic.

1 Introduction

Cysteamine hydrochloride, 2-aminoethanethiol hydrochloride ($C_2H_7NS\cdot HCl$, M = 113.61 g mol^{-1}) (Figure 1), is the salt formulation of the decarboxylated form of the amino acid cysteine and it is an important intermediate in the alternative pathway of taurine biosynthesis.[1, 2]
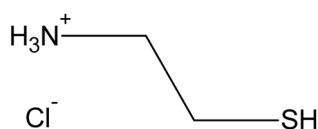
Figure 1. Chemical structure of cysteamine hydrochloride

Besides its various pharmacological effects involving the immune-reactive somatostatin levels, the secretion of several pituitary hormones, the duodenal ulcer, and also protection against oxidizing radiation, it is known to be a post-toxicant therapeutic agent for hepatic necrosis.[1, 2] Clinically, cysteamine hydrochloride is used in the treatment nephropathic cystinosis, a rare autosomal recessive disease characterized by an excessive intra-lysosomal cystine accumulation due to a defect of the transport system in the lysosomal membrane.[3, 4] Cysteamine cleaves the disulfide bond with cystine to produce molecules that can be carried out of the lysosome by a lysine carrier and thus avoid the metabolic defect in cystinosis and cystinuria.[5] Recently, the European Commission has granted orphan designation to Lucane Pharma SA, France, for cysteamine hydrochloride for the treatment of cystinosis (EU/3/14/1314). Other treatments under study are against Huntington's disease, nonalcoholic fatty liver disease, malaria, and cancer.[3]

Two crystal structures have been published in the literature;[6, 7] details can be found in Table 1. A triclinic form was observed by single crystal X-ray diffraction at 145 K with crystals obtained from 1-butanol after two weeks of crystallization at 4°C (277 K).[6] According to the authors isopropanol and n-propanol could be employed too.[6] A monoclinic form was reported in 2010.[7] The crystal had been found in the commercial sample and measured as such by single

crystal X-ray diffraction at 173 K.[7] No information on the phase relationships between these two solid forms has been provided. Lahiani-Skiba et al. mention a melting point for cysteamine hydrochloride of 70.2-70.7 °C (343.6 K) for a sample obtained from the Parisian hospitals without mentioning the crystal structure.[8] The melting data gathered by Scifinder® (30 April 2014) leads to an average melting point of 69.7 °C (342.8 K) ranging from 64 up to 72 °C. No phases have been specified. To facilitate the discussion below, the following nomenclature is proposed: form I, monoclinic structure, and form II, triclinic structure (Table 1).

Table 1. Crystal structure data for cysteamine hydrochloride in the literature[a]

Space group	T (K)	$V_{unit\ cell}$ (Å^3)	Z	$v_{specific}$ (cm^{3}g^{-1})	Ref
Triclinic P-1, form II	145	558.6	4	0.7402	[6]
Monoclinic $P2_1/c$, form I	173	560.60	4	0.7429	[7]

[a] The CIF files of the structures of cysteamine hydrochloride can be found in the Cambridge Structural Database (CSD) by the reference code XIJKIK

To prepare a suitable dosage form, the physical properties of the active pharmaceutical ingredient are important information. As is clear from the foregoing, at least two phases exist for cysteamine hydrochloride; however, no information on their phase relationships has been reported, i.e. it is not known which of the two forms is the stable one at room temperature, because both structure determinations by X-ray have been carried out far below room temperature. In addition, little is known about the effect of humidity on cysteamine and whether this should be taken into account in the dosage form design. Therefore, in the present paper, a number of experimental approaches have been used to study the solid-state behavior of cysteamine hydrochloride and to report on its phase behavior as a function of pressure, temperature and humidity.

2   Experimental

2.1   Materials

Cysteamine hydrochloride was purchased from Sigma Aldrich (>98%) and used as such. Because of its hygroscopicity, samples have been prepared in a glove box with a controlled humidity of less than 10%.

2.2   Thermogravimetry

Thermogravimetry (TGA) was carried out at various rates with a TGA50 thermobalance from TA-Instruments. No weight loss was observed in the range of 25 up to 100°C.

2.3   Differential scanning calorimetry

Differential scanning calorimetry (DSC) experiments were performed on a Q100 analyzer from TA Instruments (New Castle, DE, USA). Different quantities (2 to 10 mg) of cysteamine hydrochloride and different heating rates from 0.1 up to 10 K min^{-1} were used. The measurements were carried out on samples sealed in aluminum pans.

2.4   High-resolution X-ray powder diffraction

High-resolution X-ray powder diffraction patterns were obtained as a function of temperature from 120 K up to the liquid state with a CPS120 diffractometer from INEL (France) equipped with a liquid nitrogen 700 series Cryostream Cooler from Oxford Cryosystems (Oxford, UK). Data were collected for at least 1 hour per diffraction pattern. The heating rate between the measurements was 1.3 K min^{-1} and before data collection the sample temperature was left to stabilize for at least 15 min. The lattice parameters as a function of temperature have been determined with Pawley fits to the known unit cells using TOPAS Academic.[9]

2.5   Crystal structure solution

For structure solution, the program *DASH*[10] and *TOPAS-Academic*[9] were employed and the powder pattern was truncated to 48.80° in 2θ (Cu $K\alpha_1$), corresponding to a real-space resolution of 1.86 Å. The background was subtracted with a Bayesian high-pass filter.[11] Peak positions for indexing were obtained by fitting with an asymmetry-corrected pseudo-Voigt function.[12, 13] 22 peaks were indexed with the indexing program DICVOL04.[14-16] A monoclinic unit cell was obtained with figures of merit M(22) = 20.4 and F(22) = 39.9 (0.0069, 80). Pawley refinement was used to extract integrated intensities and their correlations, from which the space group was determined using Bayesian statistical analysis.[17] The space group $I2/a$ was returned as the most probable option, which was the space group with the highest symmetry. It resulted in a Pawley χ^2 of 5.23. Simulated annealing was used to solve the crystal structure from the powder pattern in direct space. The starting molecular geometry was taken from the published monoclinic structure (form I) from the CSD (reference code XIJKIK01).[18] In all 30 simulated annealing runs, the same crystal structure was found. The profile χ^2 of the best solution was 19.37, which is about four times the Pawley χ^2; these are good indications that the correct solution has been found.

2.6 Rietveld refinement

For the Rietveld refinement, data out to 71° 2θ were used, which corresponds to 1.33 Å real-space resolution. The Rietveld refinement was carried out with *TOPAS-Academic*.[9] Bond lengths, bond angles and planar groups were subjected to suitable restraints, including bonds to H atoms, based on the distances found in the structure XIJKIK01. A global B_{iso} was refined for all non-hydrogen atoms, with the B_{iso} of the hydrogen atoms constrained at 1.2 times the value of the global B_{iso}. The inclusion of a preferred-orientation correction with the March-Dollase formula[19] was tried for several directions, leading to an improved R_{wp} (4.581 versus 5.0) for the direction (3 1 0). The molecular geometry was checked with *Mogul*,[20] which compares each bond length and bond angle to corresponding distributions from single-crystal data. Supplementary crystallographic data can be found in the CCDC, deposit number 1027495 and obtained free of

charge from the Cambridge Crystallographic Data Centre via www.ccdc.cam.ac.uk/data_request/cif/.

2.7 High-pressure thermal analysis

The transitions observed by DSC have been studied with high-pressure differential thermal analysis (HP-DTA). An in-house constructed HP-DTA, similar to the apparatus previously built by Würflinger[21] with temperature and pressure ranges from 203 to 473 K and 0 to 300 MPa, respectively, was used. Samples were sealed in cylindrical tin pans and to ensure that in-pan volumes were free from residual air, specimens were mixed with an inert perfluorinated liquid (Galden® from Bioblock Scientifics, Illkirch, France) before sealing. HP-DTA scans were carried out with a heating rate of 2 K min^{-1}. In addition, DSC runs at ordinary pressure (i.e., in standard aluminum pans) with mixtures of cysteamine hydrochloride and perfluorinated liquid were carried out to verify that the latter was inert.

2.8 Differential vapor sorption

Differential vapor sorption (DVS) experiments have been carried out on a DVS-1000 of Surface Measurement Systems (SMS) London, UK. About 10 mg of cysteamine hydrochloride has been used in each experiment and relative humidities ranged from 0 to 90 %. The sample was considered stable with respect to the imposed water vapor once the fluctuation of its mass was below 0.001 mg.

2.9 Thermal expansion of the crystals

To investigate the thermal expansion of the crystal structures, all diffraction patterns belonging to a single series of measurements have been refined together in *TOPAS-Academic*[9] using Rietveld refinement of the known monoclinic structure with globally defined atom coordinates. In addition, the diffraction parameters such as the zero error and the slid width have each been refined with single variables for all patterns together. The unit cell parameters and peak shape parameters were allowed to refine freely.

The anisotropy of the intermolecular interactions can be investigated with the isobaric thermal expansion tensor, which is a measure of how the interactions change with temperature.[22] A small value for a tensor eigenvalue is commonly referred to as a "hard" direction and a large value as a "soft" direction.[23] The tensor has been calculated with the program PASCAL[24] and drawn with the program Wintensor.[25]

3 Results

3.1 Thermal behavior

Two endothermic thermal events have been observed for the commercial sample of cysteamine hydrochloride. The melting peak has an onset at 340.4 ± 0.5 K (67.3 °C) with a melting enthalpy of 141.6 ± 6.7 J g^{-1} (Figure 2). Below the melting peak, another thermal event can be observed at around 322 K (49°C). The enthalpy change associated with this thermal event equals 9.9 ± 1.8 J g^{-1}. Cooling down directly after the appearance of the small peak does not lead to any exothermic events and on reheating the small peak does not reappear (Figure 2). After melting and recrystallization at ambient temperature, only the melting peak is observed on reheating with comparable onset temperature and melting enthalpy (Figure 2). The small peak depends on the heating rate of the DSC as can be observed in the inset of Figure 2. At low scanning rates, 0.1 K min^{-1}, it tends to a minimum value of 310 K (37 °C). As thermogravimetric measurements demonstrated that the compound exhibits no weight loss on heating, the small peak is not related to any solvent or water loss. In the next section, it will be shown that this thermal event is linked to a solid-solid phase transition.
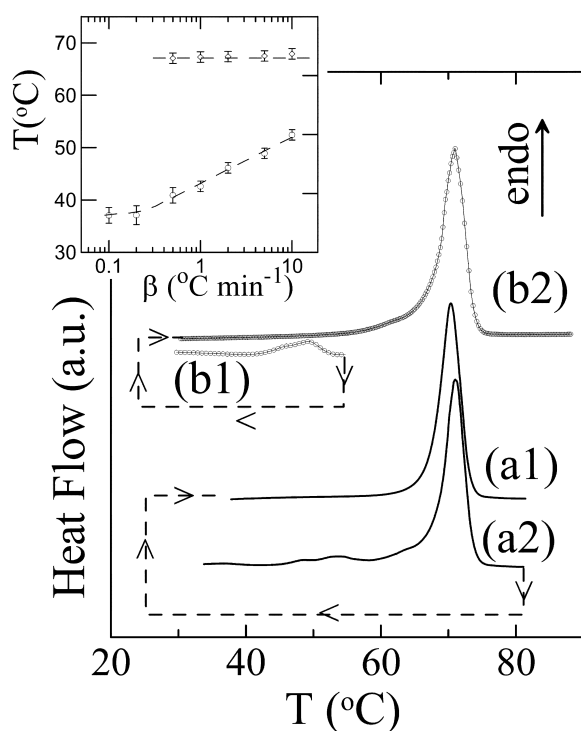
Figure 2. Thermal behavior of commercial cysteamine hydrochloride. The commercial form melts after a small thermal event **(curve a2).** The small peak does not reoccur after cooling the molten sample and reheating **(curve a1)**. Neither does it reappear after cooling just after the small peak **(curve b1 and b2)**. The inset shows the onset temperature of the small peak (open circles) and the peak of fusion (open diamonds) as a function of the heating rate. The onset temperature of the small peak levels off at 310 ± 1 K (37 °C).

3.2   Structure resolution and thermal expansion

3.2.1 Comparison of X-ray powder diffraction patterns obtained at different temperatures

At room temperature, the X-ray diffraction pattern of the commercial form clearly coincides with that of the known monoclinic form (Figure 3), called form I in the introduction. On passing 310 K, a change in the diffraction pattern can be observed, indicating that the crystal structure has changed (Figure 3a). A small change can already be observed in the pattern obtained at 310

K just below 25° 2θ. The new crystal structure is neither the known monoclinic form nor the triclinic form as can be seen in figure 3b for a pattern of the new form obtained at 200 K. This new crystalline form will be called form III from here on. The transition temperature observed by X-ray diffraction is in accordance with the temperature observed for the small peak by DSC, for which the minimum was found to be 310 K.
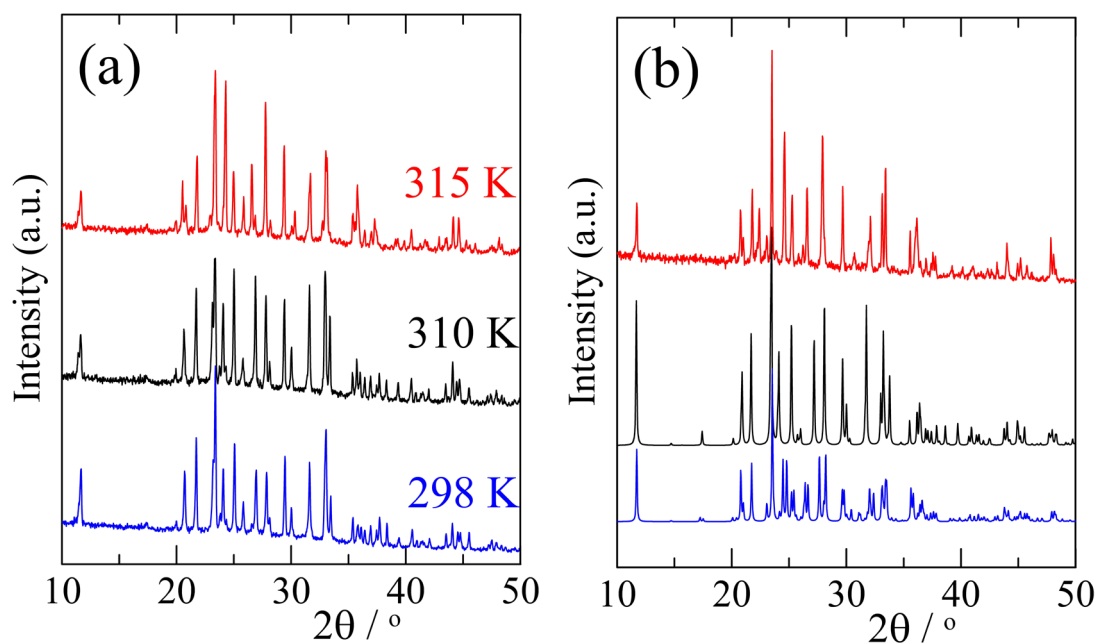

Figure 3. (a) Change in diffraction pattern between the commercial form (form I) at RT (bottom), at 310 (center) and after transition at 315 K (top). **(b)** Calculated diffraction patterns of the published triclinic (bottom) and monoclinic (center) forms with the diffraction pattern obtained by heating up to 318 K and subsequently cooling to 200 K (the peak at 22° 2θ is due to ice formation during the acquisition (top)

During the X-ray diffraction study of form III as a function of temperature, form III turned into the known triclinic form, form II, below 200K, which reverted back to form III above 200K, after which form III persisted up to the melting point. Nonetheless, a precise transition temperature for II-III has not been obtained.

3.2.2 Crystal structure resolution of the new form III

The Rietveld refinement produced a fit with $\chi^2 = 2.604$, $R'_p = 18.072$, $R'_{wp} = 16.711$ (values after background correction), $R_p = 3.195$ and $R_{wp} = 4.581$ (values before background subtraction). B_{iso} refined to 2.98(14) Å². The high value of the R values is probably due to some disorder, as the new phase forms fairly close to its melting point. The structure is monoclinic, space group $I2/a$ and a unit-cell volume of 1143.00(6) Å³. The cell parameters can be found in Table 2. A graph of the Rietveld refinement is presented in Figure 4a and the crystal packing is presented in Figure 4b.

a

b
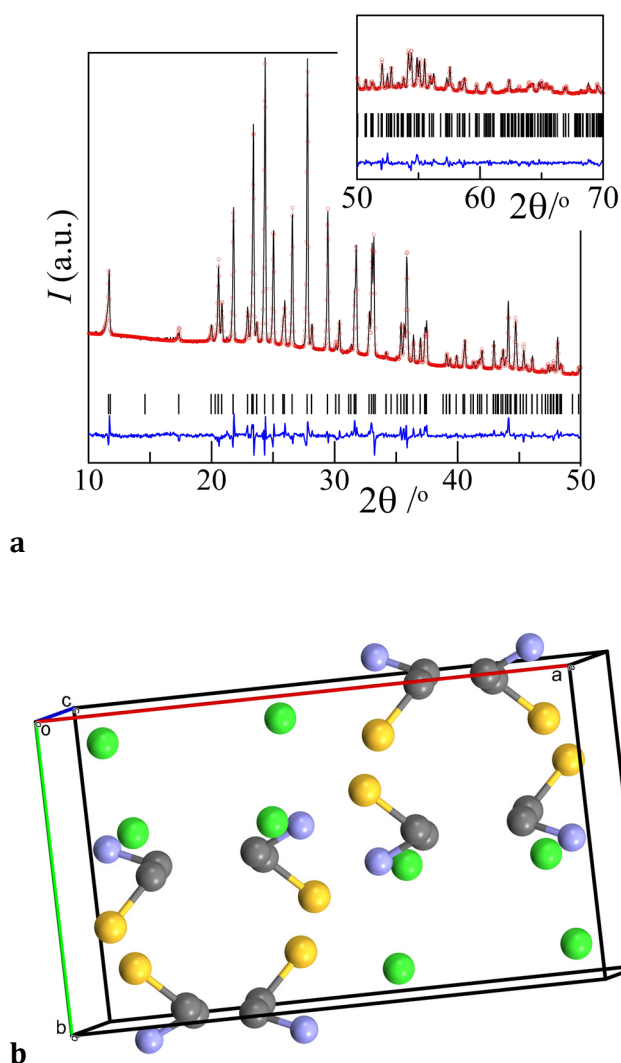
Figure 4. (a) Rietveld refinement (line) of the X-ray scattering data (open circles) of form III with residuals and diffraction lines and **(b)** The crystal packing of form III.

Table 2. Crystal Data and Structure Refinement of Cysteamine Hydrochloride Form III

Crystal data

$C_2H_8NS^+$, Cl^-

$M_r = 113.61$ g mol^{-1}

CCDC nr. 1027495

Monoclinic, $I2/a$

$a = 15.5222(5)$ Å

$b = 8.6384(3)$ Å

$c = 8.7007(3)$ Å

$\beta = 101.556(2)°$

$V = 1143.00(6)$ Å^3

$Z = 8$

$D_x = 1.32$ g cm^{-3}

Cu $K\alpha_1$ radiation

$\mu = 1.3$ mm^{-1}

$T = 293$ K

Specimen shape: cylinder 10×0.5 mm

Data collection

Diffractometer INEL CPS 120

Specimen mounting: Lindemann glass capillary 0.5 mm

Specimen mounted in transmission mode

Scan method: curved detector

Absorption correction: none

$2\theta_{min} = 5.0°$, $2\theta_{max} = 71.0°$

Increment in $2\theta = 0.029°$

Refinement

Refinement on I_{net}

$R_p = 3.195$

$R_{wp} = 4.581$

$R_{exp} = 1.760$

$\chi^2 = 2.604$

Profile function: modified Thompson-Cox-Hastings pseudo-Voigt

259 reflections

90 parameters

30 restraints

H-atom parameters restrained

Weighting scheme based on measured s.u.'s $w = 1/\sigma(Y_{obs})^2$

$(\Delta/\sigma)_{max} = 0.001$

Preferred orientation correction: March-Dollase with direction (310) and a March-Dollase parameter of 1.11

3.2.3 *Temperature dependence of the unit cell volumes of the different solid phases*

The powder diffraction patterns of the commercial cysteamine hydrochloride sample have been fitted to the known monoclinic unit cell, form I, from 120 to 310 K. From the data in Table SI.1 (Supporting Information) and the fact that $Z = 4$,[7] it follows that the specific volume of form I, $v_I(T)$ in cm^3g^{-1}, as a function of the temperature in K can be written as:

$$v_I(T) = 0.7320(17) + 3.1(1.6) \times 10^{-5}\,T + 1.9(4) \times 10^{-7}\,T^2 \tag{1}$$

This expression has an overall standard deviation of 4.2×10^{-4} $cm^{-3}g^{-1}$ for the temperature interval considered and a correlation coefficient of 0.997. In the diffraction patterns of form I as a function of temperature, no other forms have been observed.

From the data in Table SI.2 and the fact that $Z = 8$, it follows that the specific volume of form III, $v_{III}(T)$ in cm^3g^{-1}, as a function of the temperature in K can be written as:

$$v_{III}(T) = 0.735(2) - 1.5(1.4) \times 10^{-5}\,T + 3.1(3) \times 10^{-7}\,T^2 \tag{2}$$

The expression has an overall standard deviation of 5.6×10^{-4} cm^3g^{-1} within the temperature range of the data points and a correlation coefficient of 0.996. The relationship was obtained with data ranging from 120 K up to 335 K; however, the diffraction patterns below 200 K were mixed patterns of forms II and III. Thus, form II is the stable form below 200 K with respect to form III, otherwise it would not have formed.

Although there is much less data on the volume of the unit cell of the triclinic structure, for the sake of comparison, the following expression can be obtained from the unit cell volume valid within the range of 120 K up to 220 K (Table SI.3, $Z = 4$):

$$v_{II}(T) = 0.737(3) - 4.3(3.4) \times 10^{-5}\,T + 4.3(1.0) \times 10^{-7}\,T^2 \tag{3}$$

with an overall standard deviation within the temperature range considered of 2.4×10^{-4} cm^{3}g^{-1} and a correlation coefficient of 0.999. Form II was still observed together with form III in a diffraction pattern obtained at 220 K in a heating run; this indicates that the transformation from II into III is slow, but that III must be the stable form at 220 K in respect to form II, otherwise it would not have appeared.

3.3 High-pressure differential thermal analysis of the I-III and melting transitions

By high-pressure differential thermal analysis, the I-III transition and melting temperatures have been measured as a function of pressure. The data is plotted in Figure 5.
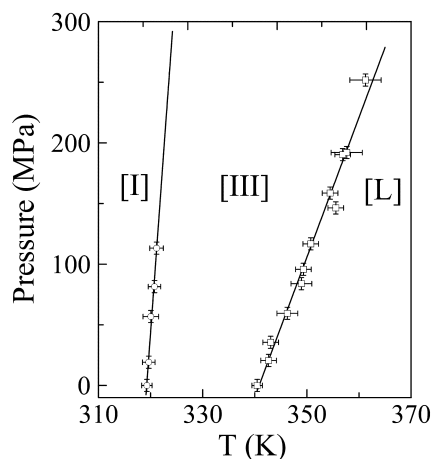
Figure 5. Transition temperature I→III (circles) and melting temperature of cysteamine hydrochloride form III (squares) as a function of the applied hydrostatic pressure.

At higher pressure, the onset temperatures of the solid-solid transition were difficult to determine in the DTA curves due to a flattened peak and low intensity and have been omitted. The data has lead to the following expressions for the equilibrium curves as a function of pressure (MPa) and temperature (K):
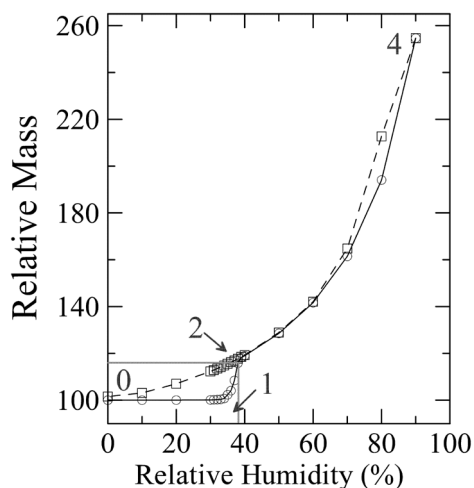
I-III: $P(T) = -19(2) \times 10^3 + 59(5)\ T$ (4)

with an overall standard deviation of 7.4 MPa and a correlation coefficient of 0.980.

III-L: $\qquad P(T) = -3.93(16) \times 10^3 + 11.5(5)\ T$ (5)

with an overall standard deviation of 10 MPa and a correlation coefficient of 0.984.

3.4 Differential vapor sorption and solubility

Figure 6. Example of a differential water vapor sorption diagram of cysteamine hydrochloride. On the vertical axis, the relative mass is given, with 100 the initial mass of dry cysteamine hydrochloride. Open circles: sorption data, open squares: desorption data. The numbers in the graph are related to Figure 14 and will be explained, when Figure 14 is discussed.

Sensitivity of cysteamine hydrochloride to water is studied by means of differential vapor sorption (DVS). As a function of the relative humidity in the system maintained at a constant temperature of 25°C, the weight of cysteamine hydrochloride has been monitored. It can be seen in Figure 6 that there is no weight change of the drug sample up to 35% relative humidity, at which it abruptly starts to take up water. Thus, cysteamine hydrochloride is not hygroscopic up to 35 % relative humidity.

Vapor pressure can be expressed by the Antoine equation, which for water in the temperature range of 273 – 303 K leads to following expression calculated by the NIST from data in the literature:[26]

$$\log_{10}(P) = 5.40221 - \left(1838.675 / (T - 31.737)\right)$$ (6)

With T in kelvin and P in bar, one finds 0.03167 bar or 3167 Pa for the vapor pressure of water at 25 °C. The water take-up of cysteamine hydrochloride starts at a relative humidity of 35%, which equals a (partial) water vapor pressure of 1108 Pa at 25°C.

Water absorption will inevitably lead to changes in the sample. It can be observed in Figure 6 that after an initial strong weight increase the curve (open circles) levels off to subsequently slowly increase the rate of absorption again. Obviously two processes are taking place in the sample, reflected by the two different trends in the same curve (open circles). The initial water uptake is either a dissolution step or the formation of a hydrate. X-ray diffraction has been used to investigate samples (form I) with different mixtures of water and cysteamine hydrochloride, however no change in the initial crystal lattice of cysteamine hydrochloride has been observed and thus the formation of a hydrate can be excluded. It implies that the initial weight gain under the presence of 1108 Pa of water pressure is a dissolution step of the solid followed by a dilution step (open circles in Figure 6; on the other hand the desorption data, open squares, represents only the dissolution behavior exhibiting hysteresis before reaching a completely dry system at 0 % RH). As dilution can only happen after saturation has been reached the crossing points of the two behaviors reflected by the open circles in Figure 6 occurs at the saturation concentration. By extrapolation, the point of intersection of the two processes occurs at a relative total mass of 117.6% and at a relative humidity of 38.3 % (or 1213 Pa partial water pressure). This leads to a saturation concentration of 0.8506 mass fraction in cysteamine hydrochloride, which is again equal to 0.4745 mol fraction in cysteamine hydrochloride, the rest being water. Clearly just a bit over 50 mole% of water molecules renders a mixture with cysteamine hydrochloride completely

liquid. This water quantity is extremely low. The proximity to the 1:1 ratio gave rise to the initial suspicion that a transitory hydrate was formed, but as stated above, X-ray diffraction did not provide any evidence for this hypothesis.

As no hydrates have been observed in the water – cysteamine hydrochloride system, its binary phase diagram must consist of a simple eutectic system. The composition of such a system as a function of temperature can be determined relatively easily by differential scanning calorimetry. Mixtures of different composition in water and cysteamine hydrochloride give in most cases rise to two peaks as a function of temperature. The lowest peak is the formation of the mixed liquid or eutectic liquid and a higher, generally shallower peak is caused by the dissolution of the remainder of the solid phase into the liquid; the highest temperature, at which the last part of the solid dissolves, is called the liquidus. A single peak is found in the binary system when its composition is exactly that of the eutectic liquid. Examples of DSC traces can be found in Figure 7 and the resulting binary phase diagram in Figure 8, in which it can be seen that the eutectic temperature is found at 240 K. In addition to the liquidus temperatures obtained by DSC, also the liquidus coordinates obtained by the DVS (the concentration of the saturated solution 0.4745 mole fraction at 298 K) have been included in Figure 8.
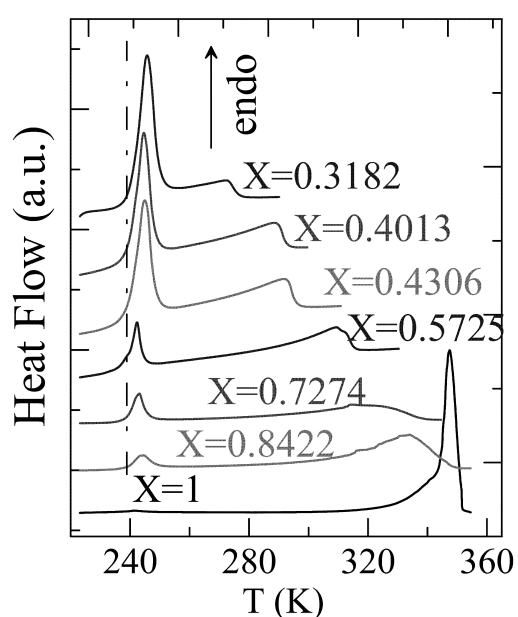
Figure 7. DSC traces of the eutectic transition and the liquidus
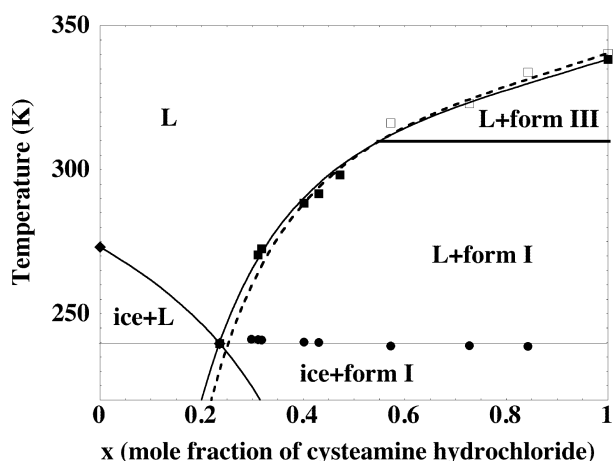
Figure 8. Temperature – composition phase diagram in mole fraction cysteamine hydrochloride in water. Measurement points and fitted lines: filled circles and hairline: eutectic temperature, filled diamond and solid curve: melting point of water with its liquidus, filled squares and solid curve: liquidus of form I, open squares and broken line: liquidus of form III. The liquidus of form III is stable above the solid – solid transition at 310 K (marked by the horizontal solid line) and the liquidus of form II is stable below 310 K. Below the eutectic temperature water and cysteamine hydrochloride crystallize in two separate solids. The liquidus lines become metastable in this domain. Liquidus curves have been fitted with the Schröder equation using a Redlich-Kister polynomial for the excess Gibbs energy; details can be found in the Supporting Information.

4 Discussion

4.1 Comparison of the new structure form III with the two known forms I and II
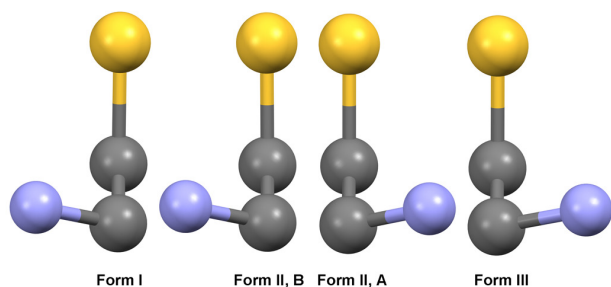
Figure 9. The different conformations of cysteamine in the three structures form I, the triclinic form II (two conformations A and B), and form III. In each case the carbon-sulfur bond is parallel to the paper.

In the results section the crystal structure of the new form III has been solved. Its structure will be compared in this section with the reported structures of forms I and II, which have been mentioned in the introduction (Table 1).[6, 7] Cysteamine has only a single torsion angle disregarding the hydrogen atoms (Figure 9). In all the 3 solid forms, the conformation of the torsion angle involving the nitrogen and the sulfur atoms is gauche. Whereas the torsion angle in form I is +61.49(15)°, in form III it is −65.2(4)°, and interestingly both torsion angles are present in form II exhibiting two separate molecules: molecule A with −60.3(6)° and molecule B with +60.7(6)° (Figure 9).

Ab initio calculations on an isolated neutral molecule of cysteamine have demonstrated the existence of 14 possible rotamers defined by the torsion angles around the C-N, C-C, and C-S bonds, the most stable having a gauche conformation around the N-C-C-S torsion, which is stabilized by an intramolecular hydrogen bond between the thiol and the amino group.[27] Although this hydrogen bond will not form with the ammonium group in cysteamine hydrochloride, in all three crystal structures the conformation around the N-C-C-S torsion angle remains gauche. That gauche is also the preferred conformation of charged cysteamine in solution is confirmed by a study of cysteamine by Raman spectroscopy.[28]

In solid form III, the asymmetric unit contains one protonated cysteamine moiety and a chloride ion, like in form I, whereas in form II *Z′* equals 2. The molecular packing of form III is presented in Figure 4b above. It consists of layers with alternating protonated cysteamine and chloride ions parallel to the *bc* plane of the unit cell. Similar layers are observed in form I and form II. Within the layers the amino groups are facing each other forming a strong square shaped hydrogen-bond motif with two chloride ions (see Figure 10). This square or slightly diamond shaped hydrogen-bond motif (graph set $R^2_4(8)$) clearly containing a strong ionic

component is approximately parallel to the diagonal of the *ab* plane of the unit cell in form III. The thiol group faces in the same direction as the amino group, thus it is the ethane backbone that interconnects the layers of molecules joined by the square-shaped hydrogen bond interaction (Figure 10) mainly by interactions between hydrogen atoms and the chloride ion. This pattern is similar in all three forms; the principal difference is the conformation of the cysteamine molecule (Figure 9).
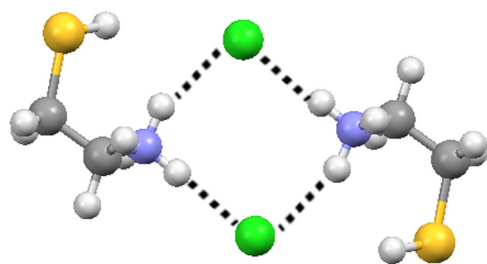
Figure 10. Square-shaped interaction pattern formed by the hydrogen bonds interconnecting the chloride ions and the NH3+ groups in form III.

In all three forms, the three protons of the terminal ammonium group are involved in hydrogen bonds with different chloride ions (Table 3). In addition, the chloride ions are also involved in weaker hydrogen-bond type interactions with CH_2 groups. This feature exists in all three structures as can be seen in Figure 11.
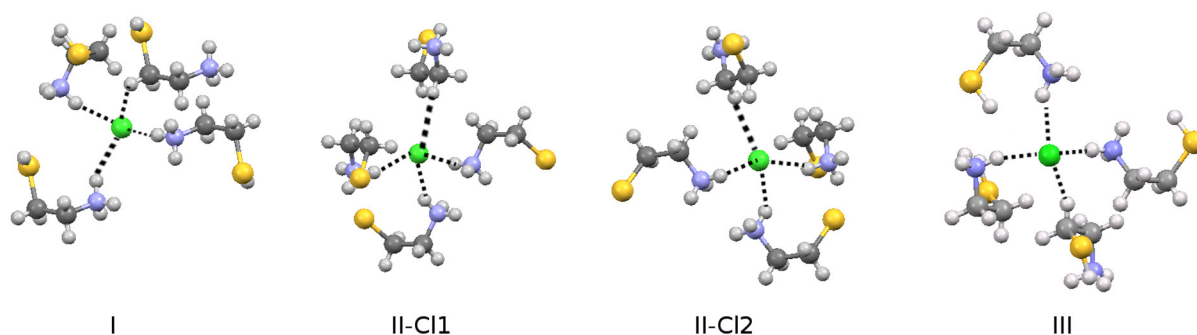
Figure 11. The coordination sphere of the chloride ion is relatively similar in the three structures. Three hydrogen bonds with the ammonium groups and one weak hydrogen bond type interaction with a C-H in the backbone of cysteamine.

Table 3. Hydrogen bonds in cysteamine hydrochloride forms I, II, and III

D-H···A	H-A	H..D	A...D	D-H...A

Form I				
N1-H1CN···Cl	0.90(3)	2.25(3)	3.1437(14)	169(2)
N1-H1BN···Cl	0.89(2)	2.44(3)	3.2563(14)	152(2)
N1-H1AN···Cl	0.89(3)	2.31(6)	3.1485(14)	158(2)
C1-H1A···Cl	0.97(3)	3.38(3)	3.8918(17)	125.9(1.8)
Form II-molecule A				
N1A-H1A5···Cl2	0.910(5)	2.2948(18)	3.135(6)	153.3(4)
N1A-H1A3···Cl1	0.910(5)	2.2569(16)	3.148(5)	166.0(3)
N1A-H1A4···Cl1	0.909(6)	2.4137(18)	3.214(5)	146.9(3)
Form II-molecule B				
N1B-H1B4···Cl1	0.910(6)	2.2857(18)	3.128(6)	153.9(4)
N1B-H1B5···Cl2	0.910(4)	2.4164(18)	3.215(4)	146.6(3)
N1B-H1B3···Cl2	0.910(5)	2.2530(16)	3.146(5)	166.7(3)
Form III				
N1-H1CN···Cl	0.91(2)	2.295(19)	3.170(5)	162.1(1.7)
N1-H1AN···Cl	0.93(3)	2.37(3)	3.208(5)	149(2)
N1-H1CN···Cl	0.93(2)	2.33(2)	3.198(5)	154.1(1.9)

C2-H2A⋯Cl	1.11(3)	2.81(3)	3.581(5)	126.8(1.7)
C2-H2B⋯S1	1.14(2)	2.90(3)	3.811(6)	136.8(1.5)

For all three forms, their thermal expansion tensors are constant over the entire temperature range. They are anisotropic exhibiting some uniaxial contraction (negative thermal expansion). The coefficients range from −13 up to 120 ×10^{-6} K^{-1} in forms I and III, which is in the same range as the thermal expansions of ternidazole, triethylenetetramine dihydrochloride and diaminopyridine phosphate.[29-31] The thermal expansion tensor for form II has been obtained with only four measurement points, as the form only appears below 200 K, hence the numerical results of the expansion tensor are most likely not accurate, however a similar picture as for the other two forms can be observed (see supporting Information Table SI.4).

In forms I and III, a small uniaxial negative thermal expansion is observed along e_1 (Table 4). This direction coincides in both crystal forms with the alignment of the ammonium groups involved in the square-shaped hydrogen-bond motif (graph set $R^2_4(8)$) with strong ionic character. The two chloride ions in this motif are more or less aligned along e_2. Considering the fact that the tensor in the e_2 direction is very similar between form I and form III (Table 4), the interactions in this direction are comparable if not similar. Projections of the thermal expansion tensor in relation to the projection of the structure have been provided in the Supporting Information (Figures SI.1-3 for forms I – III respectively).

Table 4. Coefficients of the thermal expansion tensors of forms I and II[a]

Coefficients ($\times 10^{-6}$ K^{-1})	
Form I	
α_{11}	-4.3(1.9)
α_{22}	69(3)
α_{33}	90(3)
Form III	
α_{11}	-13(4)
α_{22}	69(10)
α_{33}	123(3)

[a]See the supporting Information for an estimate of the thermal expansion tensor of form II and the orientations of the tensors (Table SI.4).

4.2 The slope of the I-III equilibrium and their volume inequality
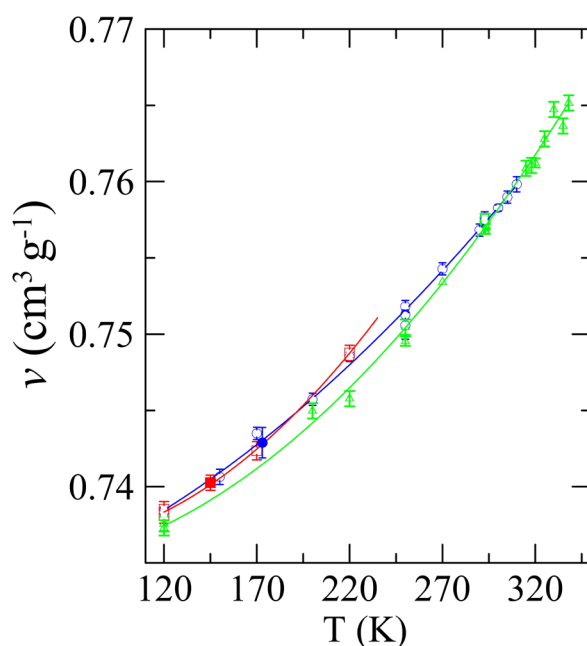
Figure 12. Specific volume of the three solid forms of cysteamine hydrochloride. Even though the measurements have been obtained by high-resolution X-ray diffraction, the volumes are so close that it is not possible to determine the sign of the volume inequalities between the three solid phases. Blue circles: form I, red squares: form II, green triangles: form III. Filled symbols are values form the literature. Lines are fits to the data.

Although the unit-cell volumes of the three solid phases have been determined as a function of the temperature with high-resolution X-ray diffraction, it has not been possible to determine the volume inequalities between the three phases (Figure 12). The volume differences are smaller than the resolution of the measurements, as is clear from the overall standard deviations provided with the fits of the specific volumes (eqs. 1-3). However, using the experimental high-pressure thermal analysis data, one can see that the slope of the I-III equilibrium is 59 ±5 MPa K^{-1} (equation (4) and Figure 5). It is also known from the DSC results that the enthalpy difference between the two solid phases equals 9.9 ± 1.8 J g^{-1}. In addition, the transition temperature has been found at 310 ± 1 K (37 °C). These values can be inserted into the Clapeyron equation to evaluate the volume difference between form I and form III:

$$\frac{dP}{dT} = \frac{\Delta S}{\Delta V} = \frac{\Delta H}{T \Delta V} \qquad (7)$$

with dP/dT the slope of a two-phase equilibrium in the pressure – temperature phase diagram in MPa K^{-1}, ΔS the entropy difference between the two phases in equilibrium, ΔV the volume inequality between the two phases in equilibrium. At equilibrium, ΔS can be replaced by $\Delta H/T$, the enthalpy difference divided by the transition temperature obtained by calorimetry.

Using expression 7, the volume difference between forms I and III can be calculated and it follows that $\Delta_{I \rightarrow III} v = 5.4(1.1) \times 10^{-4}$ cm^{-3}g^{-1}. This implies that the volume difference going from form I to form III is positive, thus form III would have a slightly larger volume than form I. However, it is also clear that the volume inequality is of the same order of magnitude as the global fitting errors of the expressions for the specific volumes of forms I and III (4.2×10^{-4} cm^{-3}g^{-1} and 5.6×10^{-4} cm^{3}g^{-1} respectively for eqs. 1 and 2). Thus, it can merely be stated that the volume change is very small and most likely positive going from form I to form III. The steep slope of the equilibrium line (Figure 5) implies that the transition is mainly heat or entropy driven, as its dependence on the pressure is very weak, which is equivalent to the observation that the volume change between the two solid phases is very small.

4.3 Pressure-temperature curve of the solid – liquid equilibrium III-L

The slope of the HP-DTA measurements equals 11.5 ±0.5 MPa K^{-1} (eq. 5). At the transition temperature 340.4 ±0.5 K (67.3 °C), the enthalpy change associated with the transition equals 141.6 ±6.7 J g^{-1}. The volume of form III is known at the melt and equals 0.766 cm^{3}g^{-1} using equation eq. 2. As in the previous section, the experimental slope of the solid – liquid equilibrium allows the calculation of the volume inequality between the liquid phase and form III, which leads to $\Delta_{III \rightarrow L} v = 0.0361$ ±0.0026 cm^{3}g^{-1}, which in turn leads to the specific volume of the liquid at the melting point, 0.802 ±0.005 cm^{3}g^{-1}. This is an increase of 4.7 % in volume on melting, which is fairly small in comparison with most pharmaceutical systems, where the average difference is in the order of 11%.[32, 33]

4.4 The topological pressure-temperature phase diagram involving form I, form III and the liquid

4.4.1 What is a topological phase diagram

A topological phase diagram is a schematic representation of the domains of the stable phases and their phase relationships. It can be extended to the metastable and supermetastable phase domains because from a thermodynamic point of view these are simply states with a higher Gibbs energy that eventually may lose their excess Gibbs energy to turn into the most stable state spontaneously. There is no rule stating in which timeframe this will occur. A well-known example is the allotropic forms diamond and graphite of which graphite is the most stable phase under ambient conditions. This has not stopped anyone from spending lots of money on the less stable diamond and neither are we concerned that diamond will convert into graphite in our lifetime.

The topological phase diagram will be constructed with as much available experimental data possible; however, in the case that data is lacking e.g. a melting point of a metastable phase or triple points under very high or negative pressure, use will be made of extrapolations and calculations, which are thermodynamically sound, even if they may be approximate. It should be kept in mind that the main goal of this topological phase diagram is to demonstrate the relative positions of the different phase domains towards each other as a function of pressure and temperature and those of the two-phase equilibria, which represent the boundaries between the domains. The more experimental data available, the more accurate will be the phase diagram; however, certain parts of it may remain approximate.

To construct the topological pressure-temperature phase diagram in the present case, the expressions of the phase equilibria between the condensed phases I-III, III-L, and the metastable I-L are needed, triple points I-III-L, I-III-V, I-L-V, and III-L-V need to be located (with L the liquid phase and V the vapor phase) and for the sake of completeness the curves representing the saturating vapor pressure of the condensed phases, the equilibrium lines I-V, III-V, and L-V. In

the present section, the necessary data will be assembled and where necessary processed with accepted thermodynamic equations to construct the topological phase diagram.

4.4.2 Phase equilibria I-III, III-L and I-L

In section 3.3, the expressions for the phase equilibria I-III (eq. 4) and III-L (eq. 5) have been determined. The expression for the metastable phase equilibrium I-L is not known however because the melting of phase I has not been observed and it will be obtained by calculation and extrapolation below.

As can be seen in Figure 5, phase equilibria of condensed phases on the pressure-temperature plane can be represented over a reasonable pressure-temperature interval as straight lines. In any case, phase equilibria are monotonously increasing functions due to the fact that the Gibbs energies involved are monotonous surfaces as a function of pressure and temperature.[34, 35] The simplest approximation of a monotonously rising function is a straight line. To obtain a linear expression for the phase equilibrium I-L, the metastable melting of form I, two points in the pressure-temperature domain need to be found on the I-L equilibrium line. The two points that will be used are I-L-V and I-III-L, two triple points containing the I-L equilibrium.

Even though the melting point of form I is not observed by DSC as it converts into form III before melting, thermodynamically the equilibrium between form I and the liquid exists as a metastable equilibrium for which the temperature can be determined using an expression obtained from thermodynamics and neglecting heat capacities[36-38]:

$$T_{I \to L} = \frac{\Delta_{III \to L}H + \Delta_{I \to III}H}{\dfrac{\Delta_{III \to L}H}{T_{III \to L}} + \dfrac{\Delta_{I \to III}H}{T_{I \to III}}} \tag{8}$$

Here $T_{I \to L}$ is the melting point of form I in kelvin, $\Delta_{III \to L}H$ is the melting enthalpy of form III and $T_{I \to III}$ is the temperature at which forms I and III are in equilibrium. The other two variables follow the same nomenclature. Using the calorimetric data presented in the results section, one

finds 338.3 K (65.1 °C), thus just below the observed melting point. Because form I is metastable at its melting point it cannot melt at a higher temperature than form III. The close proximity of the two melting points justifies neglecting the heat capacities.[37]

The pressure at the melting temperature will depend on the vapor pressure of the condensed phases of the I-L equilibrium in the DSC pan. Because the available volume in sealed DSC pans is small, the saturated vapor pressure will be quickly reached; thus, the melting transition, implying the equilibrium between solid I and the liquid occurs in equilibrium with the vapor phase and this is therefore a triple point, in the present case I-L-V. The vapor pressure of solid or liquid cysteamine hydrochloride has not been measured to our knowledge, but because it is a salt, it must be very low, not higher than a few pascal and most likely lower. Thus the coordinates of the triple point I-L-V can be considered to be approximately 338 K, 1 Pa.

The second triple point that will be used to determine the position of the I-L equilibrium line is I-III-L. It can be seen that equilibria I-III and III-L must intersect at this triple point too. Because the expressions for the latter two equilibria are known (eqs. 4 and 5), setting those expressions equal to each other allows to find the temperature of the triple point and the pressure follows from either eqs. 4 or 5. This leads to the coordinates 314 K, −309 MPa. Obviously, these coordinates are obtained by approximation using straight lines and their values are not accurate, however, they suffice to obtain an expression for the two-phase equilibrium I-L. It can be observed that the pressure of the triple point is negative. One should be aware that in these calculations negative pressure is mainly used as a mathematical approach; however negative pressure is a physical reality as can be judged from the following references.[34, 39, 40]

With the forgoing coordinates obtained for the triple points I-III-L and I-L-V a straight line can be fitted and the following approximate expression for the I-L equilibrium in the pressure – temperature phase diagram can be obtained:

I-L: $\qquad P(T) = -4.3 \times 10^3 + 12.8\,T$ $\qquad\qquad\qquad\qquad\qquad$ (9)

Assuming that the specific volume of the melt does not change much within the two degrees difference between the two melting points (I-L 338 K, III-L 340 K), the volume inequality between form I and the liquid can be obtained, $\Delta_{I \to L}v$ = 0.0376 cm³g⁻¹ (the melting point of form I together with eq 1 results in the specific volume of form I, 0.7641 cm³g⁻¹. The specific volume of the melt was obtained in section 4.3). With the slope of the I-L equilibrium (eq. 9), the volume inequality and the transition temperature, the enthalpy of transition for the melt of form I can be obtained, which leads to $\Delta_{I \to L}H$ of 162 J g⁻¹. This compares to an enthalpy of 151 J g⁻¹, if a thermodynamic cycle (Hess' cycle) is used; the enthalpy, a state function, must fulfill $\Delta_{I \to L}H$ = $\Delta_{I \to III}H$ + $\Delta_{III \to L}H$, because on both sides of the equality sign the initial state and the final state are the same (form I and the liquid, respectively). The difference between the melting enthalpies obtained via the two approaches (topological or Hess' cycle) is 7%; this demonstrates that even though some of the calculations above are based on extrapolations and approximations, the obtained topological results are consistent with the results of the Hess' cycle.

Using eqs. 4, 5, and 9 a topological phase diagram has been constructed (Figure 13). The triple point I-III-L is the point where the three equations intersect. The triple points I-III-V, I-L-V, and III-L-V are the solid-solid transition, the metastable melting point of form I and the stable melting point of form III under saturating vapor pressure of cysteamine hydrochloride. These three triple points reflect the conditions in DSC measurements as stated above when discussing the I-L-V triple point. Their coordinates are therefore respectively 310 K, 338 K and 340 K, with a vapor pressure that will slowly rise with temperature, but remain low (in the order of a few Pa) due to the fact that cysteamine hydrochloride is a salt. To reflect the increase of the vapor pressure, and also the fact that each condensed phase has its own vapor equilibrium, a schematic representation of the I-V, III-V, and L-V equilibrium curves have been added to Figure 13. The exact vapor pressure they represent is not known, but their relative position in the pressure-temperature phase diagram follows a well-established order.[37, 41]

One of the questions a topological phase diagram helps to answer is what is stable and under which conditions for the phases present in the phase diagram. This analysis is purely based on thermodynamics. First of all the III-L equilibrium line and the triple point III-L-V are stable, because they represent the highest melting solid and order → disorder transitions are not kinetically restricted. Around triple points equilibrium lines must obey the alternation rule. It signifies that an equilibrium crossing a triple point becomes metastable in relation to another phase, which becomes more stable and it means that around a triple point one will find alternatingly stable and metastable equilibrium lines. Thus around III-L-V, III-L is stable (black solid line) with increasing pressure and metastable (gray broken line) below the triple point where the vapor phase is more stable. On the left hand side of the triple point the stable III-V equilibrium is found, which, passing through III-L-V, becomes metastable, where the liquid phase is the more stable phase. Inversely, a stable L-V equilibrium is found on the right-hand side, which becomes metastable on the left-hand side (difficult to see due to the presence of triple point I-L-V), where form III is the most stable phase.

From this point on the alternation rule can be used to define the entire stability hierarchy in the topological phase diagram. As can be seen, the metastable extension of the III-L equilibrium crosses the extensions of the I-L and I-III equilibria at negative pressure. The alternation rule implies that I-L must have a different ranking from III-L and I-III, which must both have the same ranking (metastable). Triple points of condensed phases under negative pressure must be metastable;[39] therefore, the only option for the stability ranking of equilibrium I-L is even less stable than III-L and I-III, so-called supermetastable (dotted line). The metastable extension of equilibrium I-III meets the stable equilibrium III-V in the triple point I-III-V, and thus this triple point is stable and the equilibrium I-III becomes stable on crossing the triple point I-III-V increasing in pressure. Triple point I-L-V on the other hand is met by the supermetastable equilibrium I-L and the metastable equilibrium L-V (through III-L-V), thus this triple point I-L-V must be metastable. The resulting topological phase diagram is presented in Figure 13 with all equilibrium lines and triple points obeying the alternation rule.

As the transition I-III is stable, both form I and form III must have a stable domain too. Because the I-III equilibrium and the III-L equilibrium are positive and diverge with increasing pressure (Figures 5 and 13) the two phases have an overall enantiotropic phase relationship.[42, 43] As for the triclinic form II (absent in this phase diagram), only the specific volume is known as a function of temperature between 100 and 200 K. The fact that II appeared at low temperature during the measurements indicates that it is more stable than form III at low temperature, but the transition temperature is not known. It is therefore not yet possible to incorporate form II in the present phase diagram. Nonetheless, the stability *hierarchy* between forms I and III determined in this paper will not be affected once form II is added to the phase diagram.
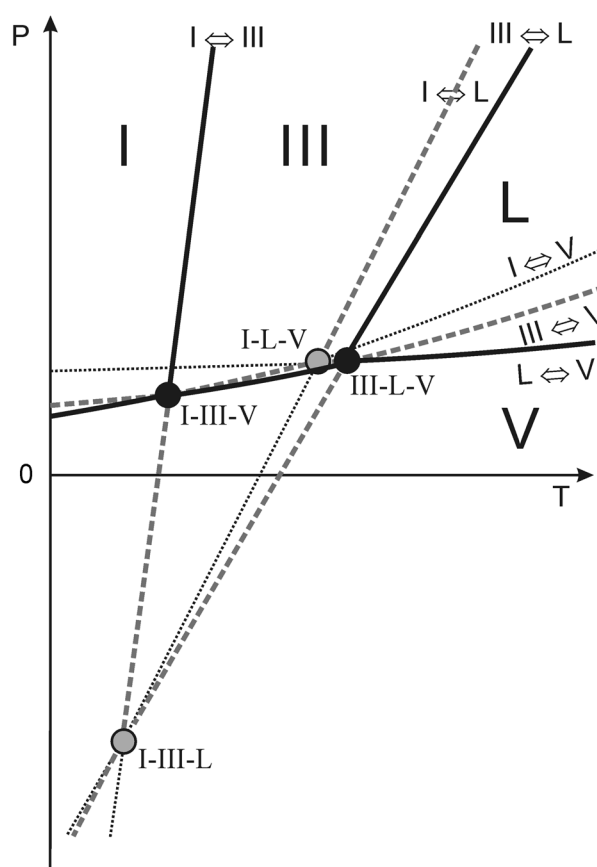
Figure 13. Topological phase diagram of cysteamine hydrochloride involving solid forms I and III. Lines: schematic representation of two-phase equilibria, solid line: stable, broken line: metastable, dotted line: supermetastable, Circles: triple points, filled circle: stable, gray circle: metastable. The stability domains of the solid forms I and III, the liquid and the vapor phase have

been marked by respectively I, III, L, and V. Their stable domains are defined by the black solid lines, which represent the stable two-phase equilibria involving the stable phases on both sides of those lines. Pressure and temperature are not to scale; the vapor pressures of all condensed phases are on this scale effectively 0 MPa. However, from a thermodynamic point of view vapor is present; therefore, the part of the pressure scale close to 0 MPa has been exaggerated to demonstrate the interchanging stability hierarchy of the different equilibria involving the vapor phase. The temperature coordinates of triple points I-III-V, I-L-V, and III-L-V are respectively 310 K, 338.3 K, and 340.4 K with an approximate but positive pressure of 0 MPa. Triple point I-III-L has the approximate coordinates of 314 K and -309 MPa.

4.5   Stability with respect to water

In the results section, it has been found that cysteamine hydrochloride forms a eutectic equilibrium with water. In principle, it is possible to calculate the entire eutectic phase diagram once the eutectic temperature and a few temperature points on the liquidus line have been obtained. However, the present system has the complication of the phase change with increasing temperature. Considering the DVS curve in Figure 6, the presence of a small amount of water vapor, does not appear to affect the state of cysteamine hydrochloride, as the water does not get absorbed (its mass remains virtually constant up to 35 %RH). Therefore solid solutions –i.e. the incorporation of water molecules in the crystal structure of cysteamine hydrochloride- probably do not exist for the present system. In that case, the liquid in the binary system saturated in cysteamine hydrochloride is in equilibrium with the pure solid state of the drug. This allows to use the Schröder equation with a Redlich-Kister polynomial to calculate the Gibbs excess energy in the liquid phase. Details of the calculations can be found in the Supporting Information.

The delicate part for this system is the phase transition between form I and form III that occurs at approximately 310 K. The eutectic temperature occurs clearly far below this temperature, which implies that it is the eutectic formed between water and form I, the commercial form, which is stable below 310 K. The Schröder equation needs the temperature of

32

fusion and the enthalpy of fusion of cysteamine hydrochloride as input, however, these should be the values of form I for the liquidus crossing the eutectic with water. The values have been obtained in the section on the topological pressure – temperature phase diagram and equal 338.3 K for the melting point of form I and 151 J g^{-1} for its melting enthalpy. Using the measured liquidus points at and below 310 K and using the requirement that both liquidi (those of water and of form I) have to meet at the eutectic temperature of 240 K, the liquidus curves can be fitted. They are represented by the solid black curves in Figure 8. The eutectic composition found in this way is 0.235 mole%.

The same Redlich-Kister excess values can be used for the liquidus of form III, because the excess is defined by the liquid mixture. As can be seen, the broken line representing the liquidus of form III starts at a melting point above that of form I, and it intersects, as expected, the liquidus curve of form I at approximately 310 K (the shallow difference in slopes does not allow a precise determination by this method, but it clearly demonstrates that the result is **_consistent_** with the transition temperature found by DSC). Finally, it can be seen that form III produces its own metastable eutectic with water, indicated by the intersection between the liquidus curve of form III (broken line) and the one of water, at a slightly lower temperature (237 K) and a slightly higher concentration in cysteamine hydrochloride (24.7 mole%) in comparison to the eutectic found for form I.

The eutectic T-x diagram, the unary pressure temperature diagram and the DVS result in Figure 6 (representing in fact a concentration as a function of the partial pressure of water or x-P diagram, cf. Figure 14b) are all different cross sections of the pressure – temperature behavior of the binary system cysteamine hydrochloride and water. Even though a T-x diagram is generally considered isobaric, the fact that the point obtained from the DVS measurement at 25°C and 0.475 mole fraction lies on the liquidus curve obtained by DSC, proves that the obtained T-x diagram in Figure 8 is actually not isobaric, because the vapor pressure of water in the system (= in the DVS and = in the DSC pan) depends on the temperature. At the cysteamine-

rich side the pressure of the system equals that of the vapor pressure of cysteamine hydrochloride (Figure 14a). At the water-rich side, the pressure of the system is determined by the vapor pressure of pure water, which is higher than that of cysteamine hydrochloride as a function of temperature. Thus, taking the pressure coordinate into account, the projected T-x diagram in Figure 8 is actually shifted in relation to the vapor pressure of the system as schematically indicated in Figure 14a. Moreover, in P-T-x coordinates the T-x slice projected on the T-x plane in Figure 8 exhibits a curvature with increasing temperature due to the increase of the combined vapor pressure of the binary system (Figure 14a).

In Figure 14a the pressure component is simplified, because a full representation cannot be clearly presented in 3 dimensions; the present P-T-x diagram is a depiction of the condensed phases neglecting the vapor phase. The related P-x behavior during the DVS measurement at 25 °C has been provided in Figure 14b. The trace of the DVS measurement has also been indicated in Figure 14a by a dotted line. In Figure 14b, it can be seen that while the water vapor pressure is increased (black-red curve from 0 - 3) there is no immediate take up of water by cysteamine hydrochloride (black-yellow trace marked 0 – 1 in the Figure 14b). This only happens when the water vapor in the DVS reaches the vapor pressure (point 3) that is in equilibrium with the saturated solution of cysteamine hydrochloride in water (point 2: 47.5 mol% cysteamine hydrochloride at 25 °C). As can be seen in the DVS curve, Figure 6, water take-up occurs very rapidly, as the system continues to form saturated solution from the water vapor. Once all solid cysteamine hydrochloride has been converted into saturated solution with water, the solution begins to dilute (trace 2 – 4), following the water vapor pressure imposed by the DVS (trace 3 – 5) in equilibrium with the solution. As the maximum relative humidity in the DVS experiment was about 90 %RH, it is obvious from the curves that the maximum 'dilute' solution (point 4, 9.3 mol%) is still rather concentrated, as the vapor pressure is much richer in water than the solution with which the vapor is in equilibrium. The concentration in the vapor phase cannot be calculated, because the vapor pressure of cysteamine hydrochloride is not known; however, it will most likely be very rich in water.
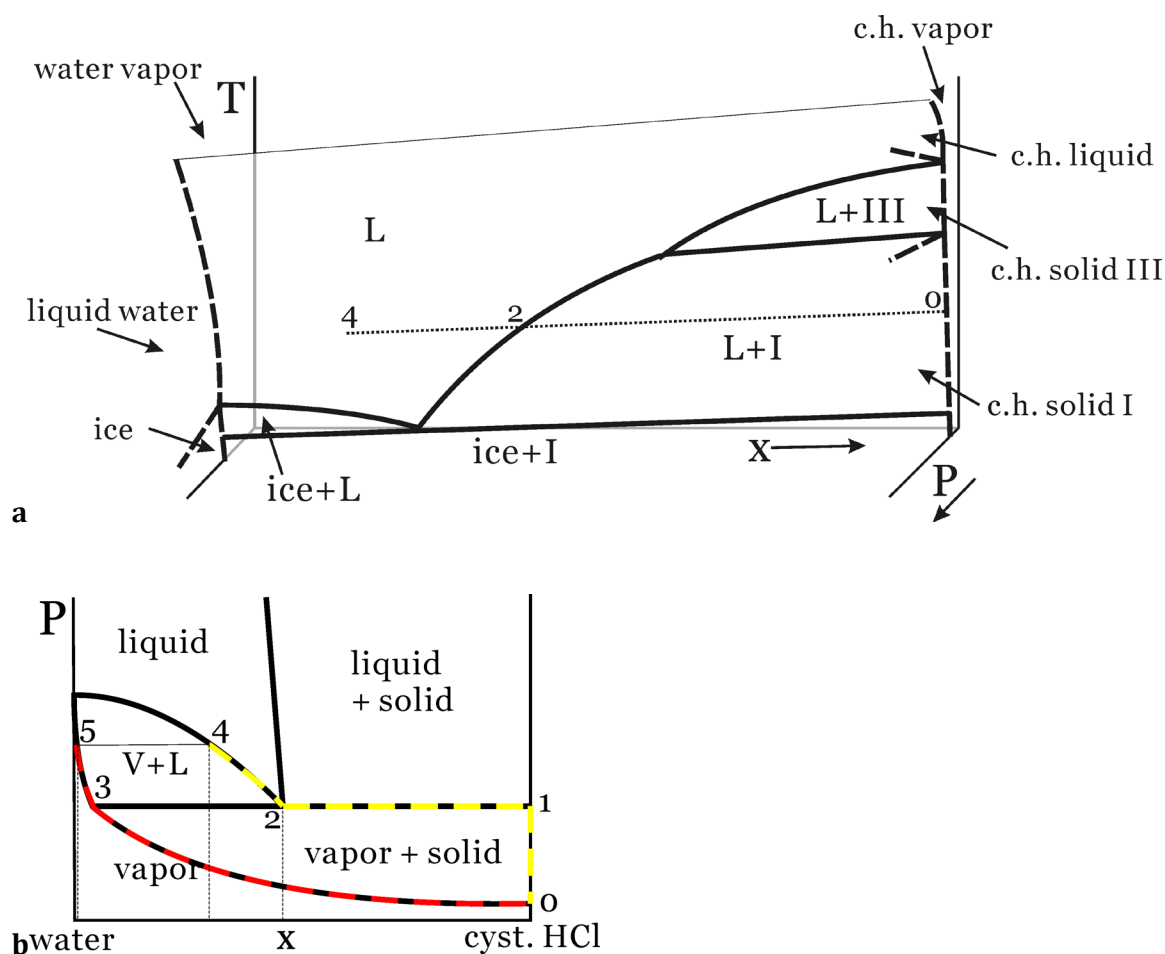
Figure 14. (a) Simplified pressure (*P*) – temperature (*T*) – composition (*x*) phase diagram for a sample under saturated vapor pressure. On the left-hand side the *T-P* diagram of water (broken lines), on the right-hand side the *T-P* diagram of cysteamine hydrochloride, marked c.h. (broken lines). The solid lines in the *T-x* diagram originate from the respective equivalent transitions in the unary *P-T* diagrams, hence also the pressure changes with the composition, as has been schematically indicated as a function of the pressure coordinate. **(b)** The real pressure – composition behavior is more complicated as is shown by the schematic P-x diagram for the DVS measurement at 25 °C (dotted line in Figure a). At point 0, bottom, right-hand side, dry cysteamine hydrochloride is subjected to water vapor. In first instance, with the increase of the water vapor pressure (red-black curve), no water is taken up by cysteamine hydrochloride (yellow-black curve) up to point 1. At point one, the water vapor pressure (3) is in equilibrium with the solid 1 and the saturated solution 2 (2 is also marked in Figure (a) and represents a

point on the liquidus curve). Increasing the water pressure leads to a dilution of the solution as indicated by the line 2-4 (cf. Figure 6, the numbers have also been provided on the DVS curve). Solution 4 is in equilibrium with vapor mixture 5 very rich in water.

5 Conclusions

A new solid form of cysteamine hydrochloride has been discovered and its crystal structure, the monoclinic spacegroup $I2/a$, has been determined by X-ray powder diffraction. All three known crystal structures of cysteamine hydrochloride have a very similar interaction make-up.

The new solid form III is stable above 310 K, but persists at lower temperatures as can be judged from the crystallographic measurements as a function of temperature down to about 200 K, as below 200 K form II appears in the diffraction patterns. The commercial form, form I, has not been observed to transform into form II at low temperature by X-ray diffraction as a function of temperature. Although this may be an indication that form I is more stable than form II at low temperature, it can simply mean that the transformation of form I into form II is slow. Forms I and III have an overall enantiotropic phase relationship or in other words, they both have a stability domain with increasing pressure. The I-III equilibrium and the III-L equilibrium diverge with increasing pressure, which implies that form I does not possess a stable melting equilibrium in the pressure – temperature phase diagram. The transition between forms I and III is mainly entropy driven, as the pressure has virtually no effect on the position of the equilibrium. Considering the reversible transition between forms III and II observed by X-ray diffraction and described in the results section, these two phases may have an enantiotropic phase relationship, although a precise transition temperature (200 ± 20 K) between the two solid phases has not been obtained. It is not clear whether form II possesses any stable domain in the P-T phase diagram, because form I, stable at room temperature, has not been observed to transform into form II at low temperatures.

It is clear that cysteamine hydrochloride is hygroscopic and water increase is substantial when the relative humidity rises above 35%. In fact above this water vapor pressure, cysteamine hydrochloride liquefies immediately to form a very concentrated saturated solution of 47.5 mole% in water. Also considering the low eutectic temperature of 240 K, it is clear that any presence of water, will basically cause cysteamine hydrochloride to dissolve. There is no evidence for the existence of a hydrate with cysteamine hydrochloride.

The present paper combines the results of measurements on the unary system with those on cysteamine hydrochloride with water. It has been shown how these different elements can be combined to improve the understanding of the system, for example for the calculation of the liquidus in the temperature – composition phase diagram.

From a pharmaceutical point of view, the findings imply that form I would be the best form to develop, as it appears to be the most stable form under ambient conditions. However, if cysteamine hydrochloride is subjected to temperatures above 40°C for a sufficient amount of time, which would only be a couple of hours, the compound may transform into form III and persist in that form when the temperature comes down to room temperature (It is not known for how long form III persists at room temperature). For formulations, this will probably have very little effect, as the volume of both phases is virtually the same. The persistence of form III under ambient conditions may however slightly increase solubilization, as form III is less stable than form I under ambient conditions.

The samples should be strictly protected against water, as a saturated solution of water and cysteamine hydrochloride forms under low water-vapor pressures. In the concentrated solution, degradation may occur among others by formation of cystamine dihydrochloride. The susceptibility to water implies that cysteamine hydrochloride should be stored in a dry environment and also that refrigeration should be avoided; cold samples will attract water by condensation and immediately form saturated solution.

Acknowledgement

Supporting Information Available

Tabulated unit cell parameters of cysteamine hydrochloride forms I, II, and III. Tabulated coefficients and orientations of the thermal expansion tensor (forms I, III, and II). Figures of the thermal expansion tensor for forms I, II, and III in relation to their respective structures. This information is available free of charge via the internet at http://pubs.acs.org/

References

1.   Kataoka, H.; Imamura, Y.; Tanaka, H.; Makita, M. Determination of cysteamine and cystamine by gas chromatography with flame photometric detection. *J. Pharm. Biomed. Anal.* **1993,** *11*, (10), 963-969.

2.   Kataoka, H.; Tanaka, H.; Makita, M. Determination of total cysteamine in urine and plasma samples by gas chromatography with flame photometric detection. *J. Chromatogr.* **1994,** *B 657*, 9-13.

3.   Besouw, M.; Masereeuw, R.; van den Heuvel, L.; Levtchenko, E. Cysteamine: an old drug with new potential. *Drug Discovery Today* **2013,** *18*, (15/16), 785-792.

4.   Labbé, A.; Baudouin, C.; Deschênes, G.; Loirat, C.; Charbit, M.; Guest, G.; Niaudet, P. A new gel formulation of topical cysteamine for the treatment of corneal cystine crystals in cystinosis: The Cystadrops OCT-1 study. *Molecular Genetics and Metabolism* **2014,** *111*, 314-320.

5.   Stachowicz, M.; Lehmann, B.; Tibi, A.; Prognon, P.; Daurat, V.; Pradeau, D. Determination of total cysteamine in human serum by a high-performance liquid chromatography with fluorescence detection. *J. Pharm. Biomed. Anal.* **1998,** *17*, 767-773.

6.   Kim, C.-H.; Parkin, S.; Bharara, M.; Atwood, D. Linear coordination of Hg(II) by cysteamine. *Polyhedron* **2002,** *21*, 225-228.

7.   Ahmad, S.; Shaheen, M. A.; Stoeckli-Evans, H. A monoclinic polymorph of cysteamine hydrochloride. *Acta Crystallogr.* **2010,** *E66*, o134.

8.   Lahiani-Skiba, M.; Boulet, Y.; Youm, I.; Bounoure, F.; Verite, P.; Arnaud, P.; Skiba, M. Interaction between hydrophilic drug and α-cyclodextrins: physico-chemical aspects. *Journal of Inclusion Phenomena and Macrocycle Chemistry* **2007,** *57*, 211-217.

9.   Coelho, A. A. *TOPAS Academic version 4.1 (Computer Software)*, Coelho Software: Brisbane, 2007.

10.   David, W. I. F.; Shankland, K.; van de Streek, J.; Pidcock, E.; Motherwell, W. D. S.; Cole, J. C. DASH: a program for crystal structure determination from powder diffraction data. *J. Appl. Crystallogr.* **2006,** *39*, 910-915.

11.   David, W. I. F.; Sivia, D. S. Background estimation using a robust Bayesian analysis. *J. Appl. Crystallogr.* **2001,** *34*, 318-324.

12.   Finger, L. W.; Cox, D. E.; Jephcoat, A. P. A correction for powder diffraction peak asymmetry due to axial divergence. *J. Appl. Crystallogr.* **1994,** *27*, 892-900.

13.   Thompson, P.; Cox, D. E.; Hastings, J. B. Rietveld refinement of Debye-Scherrer synchrotron X-ray data from Al_2O_3. *J. Appl. Crystallogr.* **1987,** *20*, 79-83.

14.   Boultif, A.; Louer, D. Indexing of Powder Diffraction Patterns for Low-Symmetry Lattices by the Successive Dichotomy Method. *J. Appl. Crystallogr.* **1991,** *24*, 987-993.

15.   Boultif, A.; Louer, D. Powder pattern indexing with the dichotomy method. *J. Appl. Crystallogr.* **2004,** *37*, 724-731.

16.   Louer, D.; Louer, M. Trial-and-Error Method for Automatic Indexing of Powder Diagrams. *J. Appl. Crystallogr.* **1972,** *5*, (Jul1), 271-275.

17.   Markvardsen, A. J.; David, W. I. F.; Johnson, J. C.; Shankland, K. A probabilistic approach to space-group determination from powder diffraction data. *Acta Crystallogr. A* **2001,** *57*, 47-54.

18.   Ilioudis, C. A.; Hancock, K. S. B.; Georganopoulou, D. G.; Steed, J. W. Insights into supramolecular design from analysis of halide coordination geometry in a protonated polyamine matrix. *New J. Chem.* **2000,** *24*, (10), 787-798.

19.   Dollase, W. A. Correction of Intensities for Preferred Orientation in Powder Diffractometry - Application of the March Model. *J. Appl. Crystallogr.* **1986,** *19*, 267-272.

20.   Bruno, I. J.; Cole, J. C.; Kessler, M.; Jie, L.; Motherwell, W. D. S.; Purkis, L. H.; Smith, B. R.; Taylor, R.; Cooper, R. I.; Harris, S. E.; Orpen, A. G. Retrieval of crystallographically-derived molecular geometry information. *J. Chem. Inf. Comput. Sci.* **2004,** *44*, 2133-2144.

21.   Würflinger, A. Differential thermal-analysis under high-pressure IV. Low-temperature DTA of solid-solid and solid-liquid transitions of several hydrocarbons up to 3 kbar. *Ber. Bunsen-Ges. Phys. Chem.* **1975,** *79*, (12), 1195-1201.

22.   Weigel, D.; Beguemsi, T.; Garnier, P.; Berar, J. F. Evolution of thermal-expansion tensor as function of temperature .1. General law of evolution of tensor symmetry. *J. Solid State Chem.* **1978,** *23*, (3-4), 241-251.

23.   Salud, J.; Barrio, M.; Lopez, D. O.; Tamarit, J. L.; Alcobe, X. Anisotropy of intermolecular interactions from the study of the thermal-expansion tensor. *J. Appl. Crystallogr.* **1998,** *31*, 748-757.

24.   Cliffe, M. J.; Goodwin, A. L. PASCal: a principal axis strain calculator for thermal expansion and compressibility determination. *J. Appl. Crystallogr.* **2012,** *45*, 1321-1329.

25.   Kaminski, W. *WinTensor (*[http://www.wintensor.com)](http://www.wintensor.com), 1.1; 2004.

26.   Bridgeman, O. C.; Aldrich, E. W. Vapor pressure table for water. *J. Heat Transfer* **1964,** *86*, 279-286.

27.   Buemi, G. Conformational analysis and rotation barriers of 2-aminoethanethiol and 2-aminoethanol: An ab initio study. *Int. J. Quantum Chem* **1996,** *59*, (3), 227-237.

28.   Riauba, L.; Niaura, G.; Eicher-Lorka, O.; Butkus, E. A study of cysteamine ionization in solution by Raman spectroscopy and theoretical modeling. *J. Phys. Chem. A* **2006,** *110*, (50), 13394-13404.

29.   Mahe, N.; Perrin, M.; Barrio, M.; Nicolai, B.; Rietveld, I.; Tamarit, J.; Ceolin, R. Solid-State Studies of the Triclinic (Z '=2) Antiprotozoal Drug Ternidazole. *J. Pharm. Sci.* **2011,** *100*, (6), 2258-2266.

30.   Mahe, N.; Nicolai, B.; Allouchi, H.; Barrio, M.; Do, B.; Ceolin, R.; Tamarit, J.-L.; Rietveld, I. B. Crystal Structure and Solid-State Properties of 3,4-Diaminopyridine Dihydrogen Phosphate and Their Comparison with Other Diaminopyridine Salts. *Cryst Growth Des* **2013,** *13*, (2), 708-715.

31.   Henriet, T. TETA. **2015**.

32.   Ceolin, R.; Rietveld, I. B. Phenomenology of polymorphism and topological pressure-temperature diagrams. *J. Therm. Anal. Calorim.* **2010,** *102*, (1), 357-360.

33.   Barrio, M.; Maccaroni, E.; Rietveld, I. B.; Malpezzi, L.; Masciocchi, N.; Ceolin, R.; Tamarit, J.-L. Pressure-temperature state diagram for the phase relationships between benfluorex hydrochloride forms I and II: A case of enantiotropic behavior. *J. Pharm. Sci.* **2012,** *101*, (3), 1073-1078.

34.   Bridgman, P. W., *The physics of high pressure*. Dover Publications: New York, 1970.

35.   Oonk, H. A. J., *Phase theory, The thermodynamics of heterogeneous equilibria*. Elsevier Scientific Publishing Company: Amsterdam, 1981.

36.   Yu, L. Inferring Thermodynamic Stability Relationship of Polymorphs from Melting Data. *J. Pharm. Sci.* **1995,** *84*, (8), 966-974.

37.   Gana, I.; Barrio, M.; Do, B.; Tamarit, J.-L.; Ceolin, R.; Rietveld, I. B. Benzocaine polymorphism: Pressure-temperature phase diagram involving forms II and III. *Int. J. Pharm.* **2013,** *456*, (2), 480-488.

38.   Bennema, P.; van Eupen, J.; van der Wolf, B. M. A.; Los, J. H.; Meekes, H. Solubility of molecular crystals: Polymorphism in the light of solubility theory. *Int. J. Pharm.* **2008,** *351*, (1-2), 74-91.

39.   Landau, L. D.; Lifshitz, E. M., *Statistical physics - Course of theoretical physics*. 3rd edition ed.; Butterworth-Heinemann: Oxford, 1984; Vol. 5.

40.   Zheng, Q.; Durben, D. J.; Wolf, G. H.; Angell, C. A. Liquids at large negative pressures: water at the homogeneous nucleation limit. *Science* **1991,** *254*, 829-832.

41.   Gana, I.; Ceolin, R.; Rietveld, I. B. Bicalutamide polymorphs I and II: a monotropic phase relationship under ordinary conditions turning enantiotropic at high pressure. *J. Therm. Anal. Calorim.* **2013,** *112*, (1), 223-228.

42.   Bakhuis Roozeboom, H. W., *Die heterogenen Gleichgewichte vom Standpunkte der Phasenlehre. Erstes Heft: Die Phasenlehre - Systeme aus einer Komponente.* Friedrich Vieweg und Sohn: Braunschweig, 1901; Vol. 1.

43.   Ceolin, R.; Tamarit, J. L.; Barrio, M.; Lopez, D. O.; Nicolaï, B.; Veglio, N.; Perrin, M. A.; Espeau, P. Overall monotropic behavior of a metastable phase of biclotymol, 2,2'-methylenebis(4-chloro-3-methyl-isopropylphenol), inferred from experimental and topological construction of the related P-T state diagram. *J. Pharm. Sci.* **2008,** *97*, (9), 3927-3941.

TOC